Geophysical Research Letters

Supporting Information for

Far-field coseismic forcing of giant rockslides in the 2017 Sarpol-Zahab Earthquake (Iran)

Aya Cheaib[1,3], Pascal Lacroix[1], Swann Zerathe[1], Denis Jongmans[1], Najmeh Ajorlou[2], Marie-Pierre Doin[1], James Hollingsworth[1], and Chadi Abdallah[3]

1. ISTerre - Université Grenoble Alpes, IRD, CNRS, IFSTTAR, Université Savoie Mont Blanc, CS 40700, 38058 GRENOBLE Cedex 9 Grenoble, France.

[2]Department of earth science, Institute for Advanced Studies in Basic Sciences(IASBS), 444 Prof. Yousef Sobouti Blvd., Zanjan 45137-66731, Iran.

[3]Lebanese National Council for Scientific Research/Remote Sensing Center, Blvrd Sport City, Bir Hassan, P.O. Box 11-8281, Beirut, Lebanon.

Contents of this file

Additional Supporting Information (Files uploaded separately)

Introduction

This document provides supplementary information on the used data and methods, the uncertainty analysis presented in the main text, an extended description of the results and detailed explanation of the giant rockslides site effect assessment.

As our study area is large and partially not well documented (Iran-Iraq boundary/area of conflict), the available geological maps were only: (1) a large geological map (1:2,500,000) for the entire Iran and (2) a 1:250,000 geological map for the Ilam province in Iran (southern far field of the earthquake). No geological maps were available for Iraq (see more details in text S1 and Figure S1).

Text S1. Data Set

Three kinds of DEMs were used in our study: (1) the ASTER GDEM of 30 m resolution (regional view of our study area), (2) 4 m resolution pre and post-earthquake DEMs (Table S1) that were generated in the region of the epicenter (Figure S1) from tri-stereo pairs of SPOT6-7 images using Ames-Stereo Pipeline (Beyer et al., 2018) , and finally (3) a 4 m resolution pre-earthquake DEM (also generated with Ames-Stereo Pipeline using tri-stereo SPOT7 images (acquired in 2014) covering the southern part of our study area, in the region of the far southern rockslides, Figure S1). See Table S1 for more details on the data.

SPOT data was provided via the CNES-funded ISIS program (now integrated with DINAMIS: Dispositif Institutionnel National d'Approvisionnement Mutualisé en Imagerie Spatiale).

The pre- and post-earthquake SPOT6-7 images (around the epicenter, Figure S1) of 1.5 m resolution were othorectified using the high resolution DEMs generated from the same data.

The PlanetScope images are available as orthorectified tiles, 10 km long and 25 km wide containing four bands (blue, green, red and infrared).

The 72 Sentinel-1 images cover 10 months before and after the earthquake. They were acquired from ESA with Interferometric Wide Swath (IW) mode from both A and B satellites and feature a 250 km swath, a spatial resolution of 5x20 m and a repeat cycle of 12 days.

A 1:2,500,000 regional geological map of the Iran republic (National Iranian Oil Company, NIOC) was used in our study, alongside a more detailed 1:250,000 geological map (Llewellyn, 1974), covering the Ilam region in Iran (Figure S1).

Text S2. Methods

Our working strategy aimed at detecting the maximum possible number of earthquake-induced landslides in our study area, extending 200+ km along the Iran-Iraq border. Thus, we used different methods: the scars of rapid coseismic landslides were mapped by a comparison of pre- and post-seismic Planet-scope images (Manual **visual comparison**), whereas slow-moving landslides (m/yr-mm/yr) were detected by deriving the ground deformation from optical (**Optical images correlation**) and radar (**Interferometric Synthetic Aperture Radar**) satellite images.

2.1. Visual comparison

To detect the rapid slope-failures, the available pre- and post-earthquake PlanetScope data were merged then compared in ArcGIS software using the **"swipe"** tool. To accomplish this inventory in the

best way, we used the available DEMs and the earth view base maps in order to verify that the detected landslide scars occur on topographic slopes and try to visualize them if possible.

2.2. Optical image correlation

The COSI-CORR iterative correlator was used to measure the horizontal displacements on the Earth's surface using georeferenced optical images (Leprince et al., 2007). Each correlation yields a north-south and an east-west displacement fields, as well as a signal to noise ratio map. It allows usually the detection of displacements higher than 10% of the image's pixel resolution during the time interval between the two correlated images.

First we correlated the mosaic of SPOT6-7 images covering the area around the epicenter (a minimum distance of 10 km and a maximum distance 75 km to the epicenter). The correlation was conducted pixel by pixel in the frequency domain using a sliding window of 64 pixels in both iterations.

In a second step we correlated the available PlanetScope images in the southern part of our study area (see Figure S1). The aim of this step is to see if we can detect any displacement fields on the body of the rockslides detected from the coseismic interferograms. Thus, the green bands were correlated in the frequency domain for each pixel using a sliding window of 64 pixels also for both iterations.

Each time, several tests were done before adopting the final sliding window sizes.

The obtained results were then detrended in ENVI software and corrected afterward with Matlab by eliminating the pixels of high signal to noise ratios then subtracting the median of all the displacement field from each pixel.

2.3. Interferometric Synthetic Aperture Radar (InSAR)

We generated differential interferograms using NSBAS (New Small BAseline Subset) (Doin et al., 2011) process chain based on the ROI_PAC software (Rosen et al., 2004). See more details in the manuscript.

Text S3. Results

In total, 369 earthquake-induced landslides were detected. We divided them into two main categories: rockfalls and giant rockslides.

3.1. Rockfalls

360 scars of rockfalls were mapped around the epicenter using the visual comparison of Planet-scope images. In the following figures we will be showing an example of how we detected the scars of the debris cones (Figure S2), their density analysis (Figure S3) and their occurrence on the available slopes (Figure S4).

3.2. Giant rockslides

9 giant rockslides were detected. One of them was the Mela-kabod rockslide detected from optical images correlation that moved coseismically for about 35 m toward the south-west (Figure S5). While 8 landslide-like patterns were detected from the coseismic interferograms (Figure 2) and then interpreted to be old giant rockslides. The characteristics of all the rockslides are detailed in Table S2 and presented in Figure S6.

However, in Ghazipur and Simpson (2016), the areas of those rockslides are systematically underestimated by up to an order of magnitude compared to the surface areas determined from our results (Table S2).

Text S4. Quantification of Giant Rockslides Coseismic Displacement

While a coseismic movement of all the rockslides is observed in the coseismic interferograms (Figure 2), its precise quantification is not possible due to (1) the sharp limits of the patterns in the coseismic interferograms, that prevent extraction of the phase ambiguity during the unwrapping process, and (2) the absence of pattern in the correlation of optical images. However, those two sources of data nevertheless provide constraints on the coseismic movement between several cm (~10 cm) in the radar LOS and 0.9 m maximum for all the rockslides (Table S2). The minimal coseismic displacement can be quantified by counting the number of fringes inside each rockslide pattern (formula: (number of fringes*wave length)/4pi). The maximum value of the coseismic displacement can be estimated by the uncertainty of the horizontal displacement field obtained from optical PlanetScope images correlation (explained above).

Text S5. Time-series analysis

After detecting and characterizing the slow movements triggered by the Sarpol-Zahab earthquake in our study area, we computed their radar LOS time-series for each pixel in the interferograms stack over 10 months before and after the earthquake. To do that, we divided the interferograms into pre- and post-earthquake groups, then we inverted the phase delays of the unwrapped interferograms pixel by pixel in order to solve the total phase delay, relative to the first date (Doin et al., 2011). Time-series were then constructed in Matlab using the cumulative deformation maps obtained from the inversion (one map at each date of the Sentinel-1 images). So we calculated the mean displacement over a selected window, of about 25x25 pixels on the landslide body at each date, relative to a mean displacement extracted from a surrounding stable area of hundreds of meters around it. The final displacement was computed from the differences between the two means. After that, the deviation

of the displacement was estimated from the mean absolute deviation of the displacement in the reference area.

In a next step, we calculated the pre-and post-seismic landslide mean velocities and their associated uncertainties. Each point "i" of the time-series is considered as a random variable of normal distribution (mu_i, sigma_i). 10,000 realizations of this random variable are randomly picked at each point of the time series, and the associated 10,000 pre and post velocities are calculated by a linear regression with time. The mean and standard deviation of these 10,000 velocities gives us an estimate of the mean velocity and its uncertainty.

Text S6. Site Effect Assessment of the Giant Rockslides

Six of the giant landslides affected the same 200 m thick Ilam formation (limestone) overlying a 100 m thick shale layer (Surgah formation). This structure constitutes a dynamic oscillator on the thick carbonate Sarvak formation.

During the slide of the rockslides, the block disintegrated and dragged part of the Surgah formation, creating a highly destructive deposit with a maximum thickness *t* of around 150 m, consisting of a mixture of shale and limestone. The amplification of the seismic waves resulting from the earthquake is due to the seismic impedance contrast (product of the density ρ and shear wave velocity *Vs*) between this deposit and the underlying, mainly calcareous, substratum. For vertically incident waves and 1D structure, the resonance frequency f_o and the corresponding amplification Af_o are given by (Kramer, 1996):

$$f_0 = \frac{Vs_D}{4\,t} \qquad (1)$$

$$Af_0 = \frac{\rho_B\, Vs_B}{\rho_D\, Vs_D} \qquad (2)$$

where Vs_D and Vs_B are the shear wave velocities of the rockslide deposit and the bedrock, respectively, and ρ_D and ρ_B are the corresponding densities.

Rockslide deposit and bedrock Vs values at these sites are not available, but plausible values can be taken from a similar rockslide for the deposit mixing limestone and marl (Socco et al., 2010) and in the literature for bedrock (Telford et al., 1990):

Vs_D= 600 m/s ; Vs_B= 3000 m/s : ρ_D= 1.9 ; ρ_B= 2.5.

Considering these values, we obtain a resonance frequency $f_o \approx 1$ Hz associated to a 1D amplification over 6.

Thus the 1D resonance frequency of the carbonate Sarvak formation before the rockslide can be estimated to be around 1 Hz, taking plausible values of dynamic material moduli. After the

rockslide, the destructured slump body, characterized by lower rigidity and smaller thickness (varying between 75 m and 150 m), also has a resonance frequency in the low range (1-2 Hz). Topographic amplification is maximum for a wavelength comparable to the width of the mountain (Geli et al., 1988), a condition that is again fulfilled in the low frequency range (around 1 Hz) if we consider a mountain a few km wide with a velocity Vs of the order of 3 km/s. These results suggest that ground motion parallel to the slope may have been significant around 1 Hz at these 6 sites during the Sarpol-Zahab earthquake, due to the combined effect of a particular directivity of the source and site amplification that can generate ground motions 5 to 10 times stronger than normal (Murphy, 2015). Interestingly, the presence of multiple ridges can even increase the topographic effect (Geli, et al, 1988).

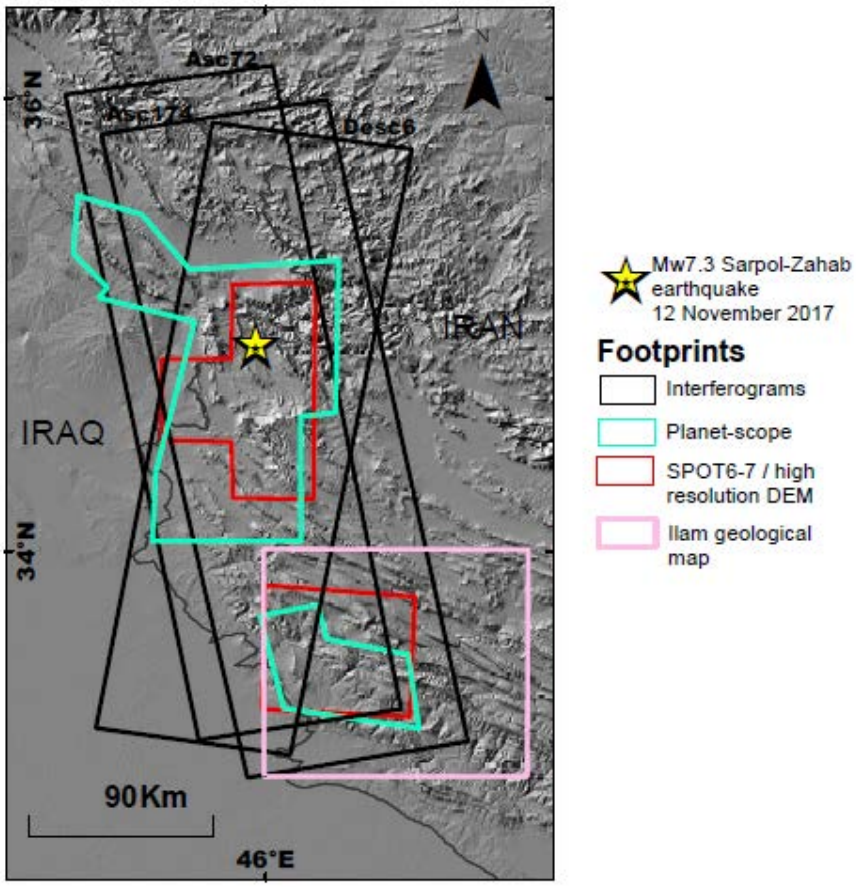

Figure S1. Footprints of the data used in our study. When pre- and post-earthquake data are available, the common area is presented.

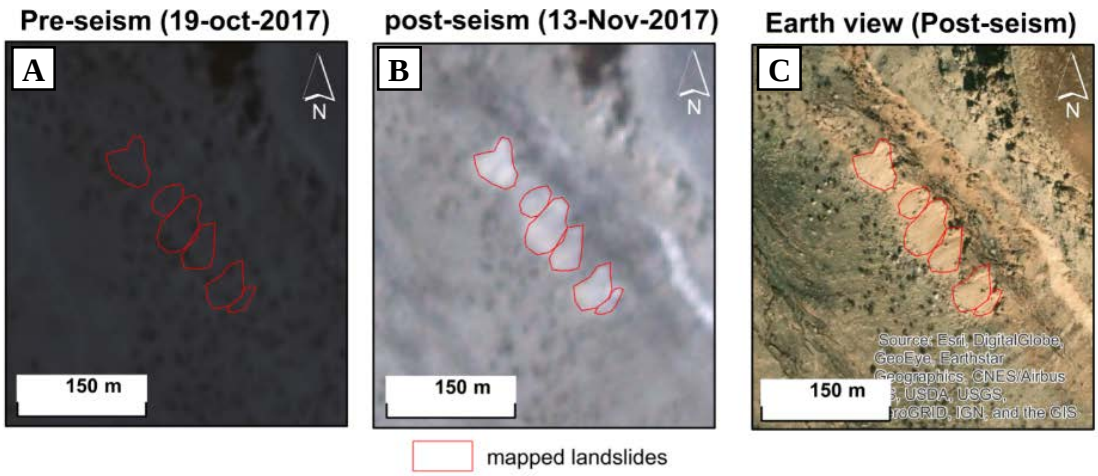

163

164 **Figure S2.** Typical example of rapid landslides mapped from PlanetScope images (3 m
165 resolution). (A) and (B) show the view of the same area from PlanetScope images before and
166 after the Sarpol-Zahab earthquake respectively. (C) shows the Google Earth view of the same
167 extent.

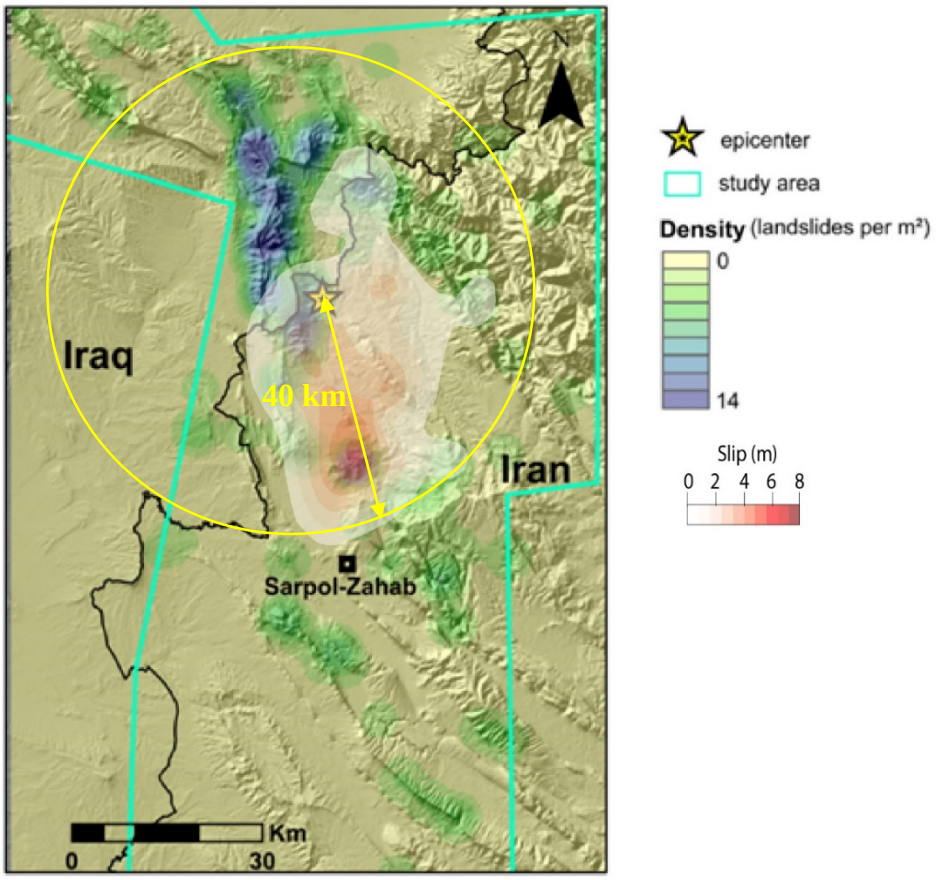

168

Figure S3. Rapid rockfalls density map. This map was calculated using the Kernel density tool in ArcGIS software by evaluating the density of points within a 5 km radius. The cumulative slip at 12 s was added from Gombert et al (2019).

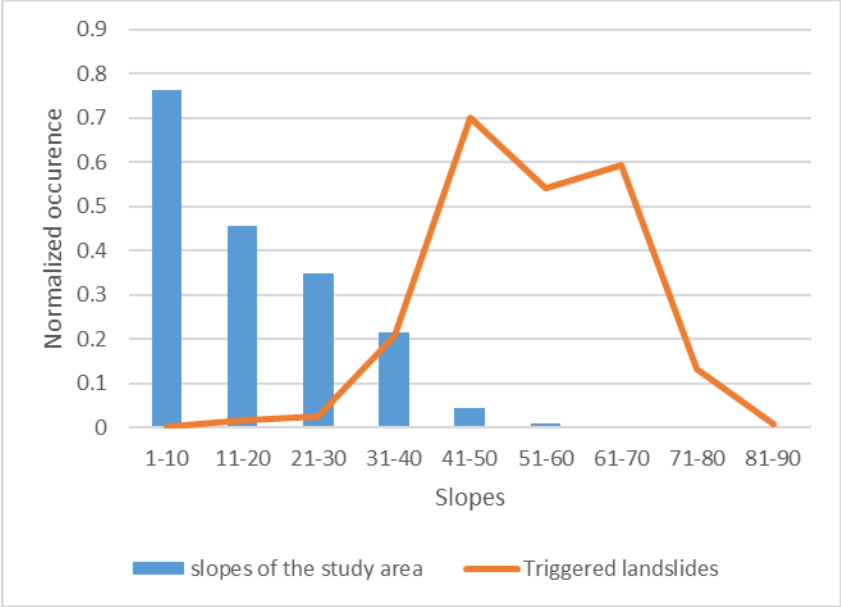

Figure S4. Plot showing the distribution of 276 detected rockfalls in respect to the available slopes of our study area.

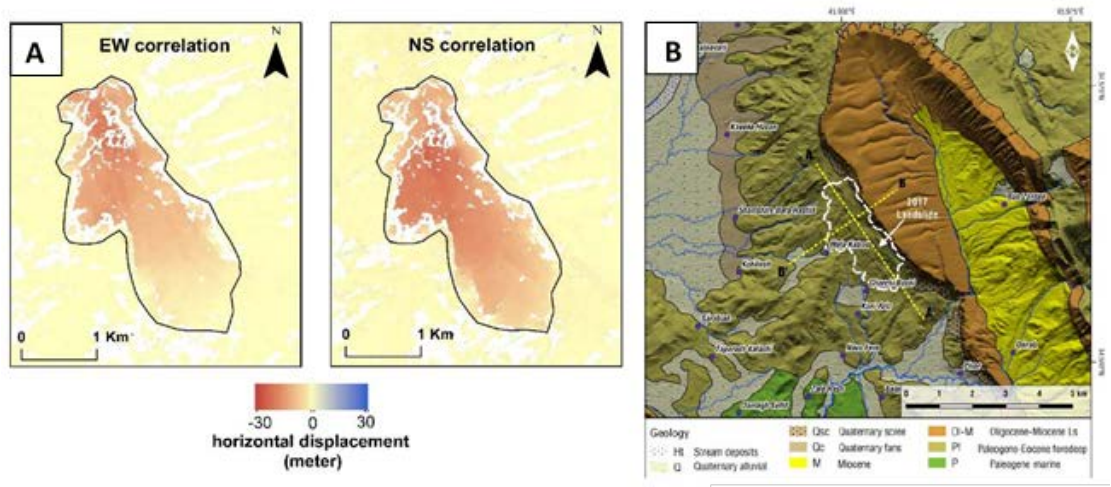

Figure S5. (A) Spot-6 images (Table S1) correlation results for the Melah-Kaboud landslide obtained using the COSI-Corr tool, showing the coseismic displacement during the Sarpol-Zahab earthquake. (B) Geological map of the Mela-Kaboud landslide region from the study of

Valkaniotis et al (2018). The white contour shows the limit of the displacement field detected from high resolution images in their study.

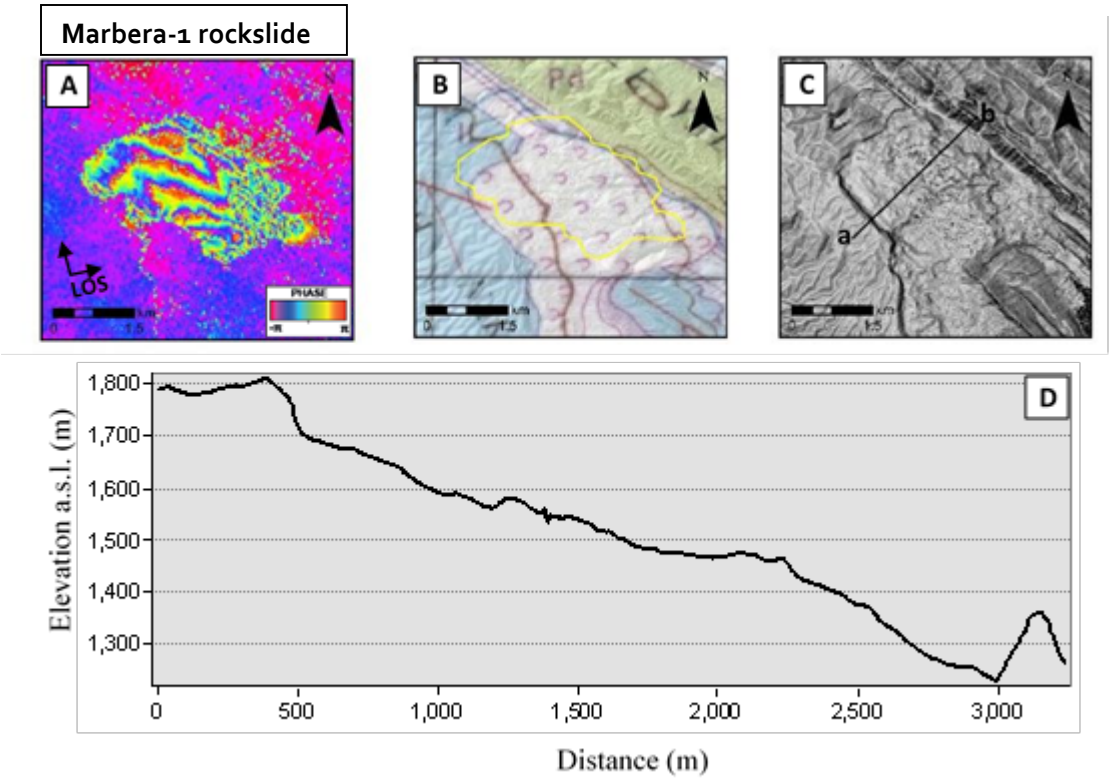

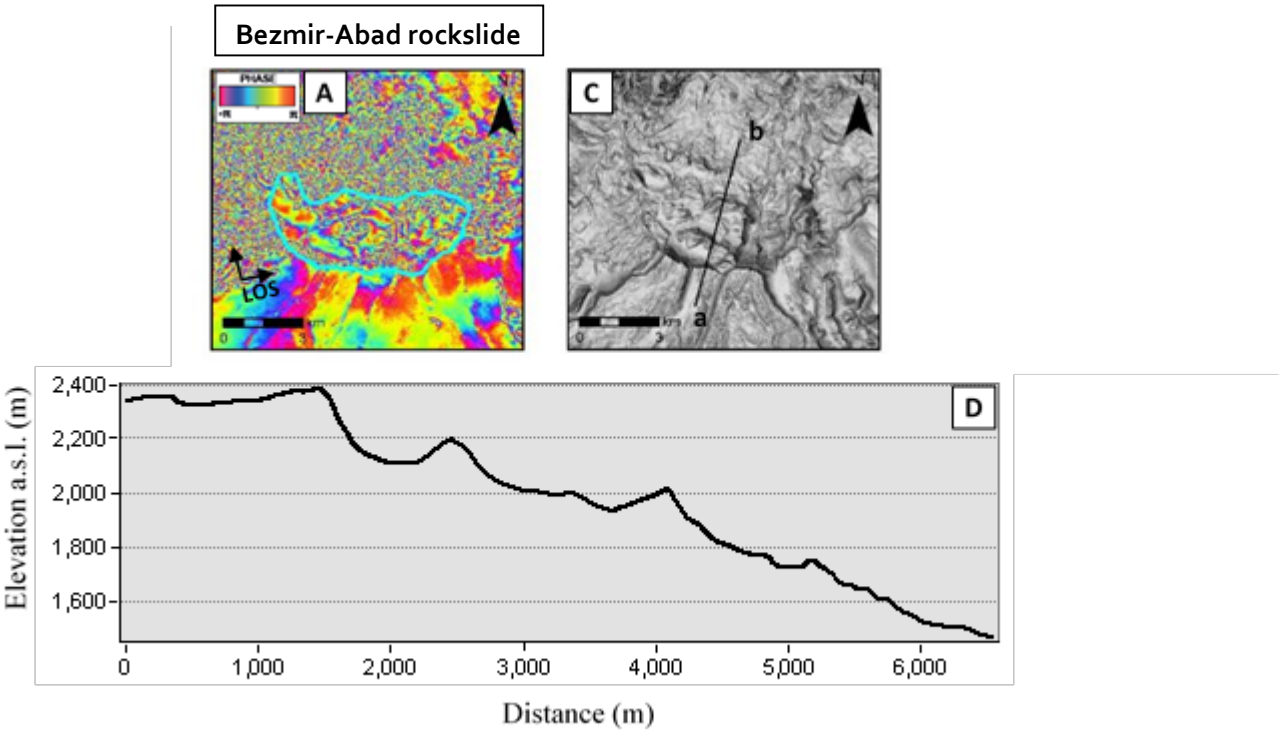

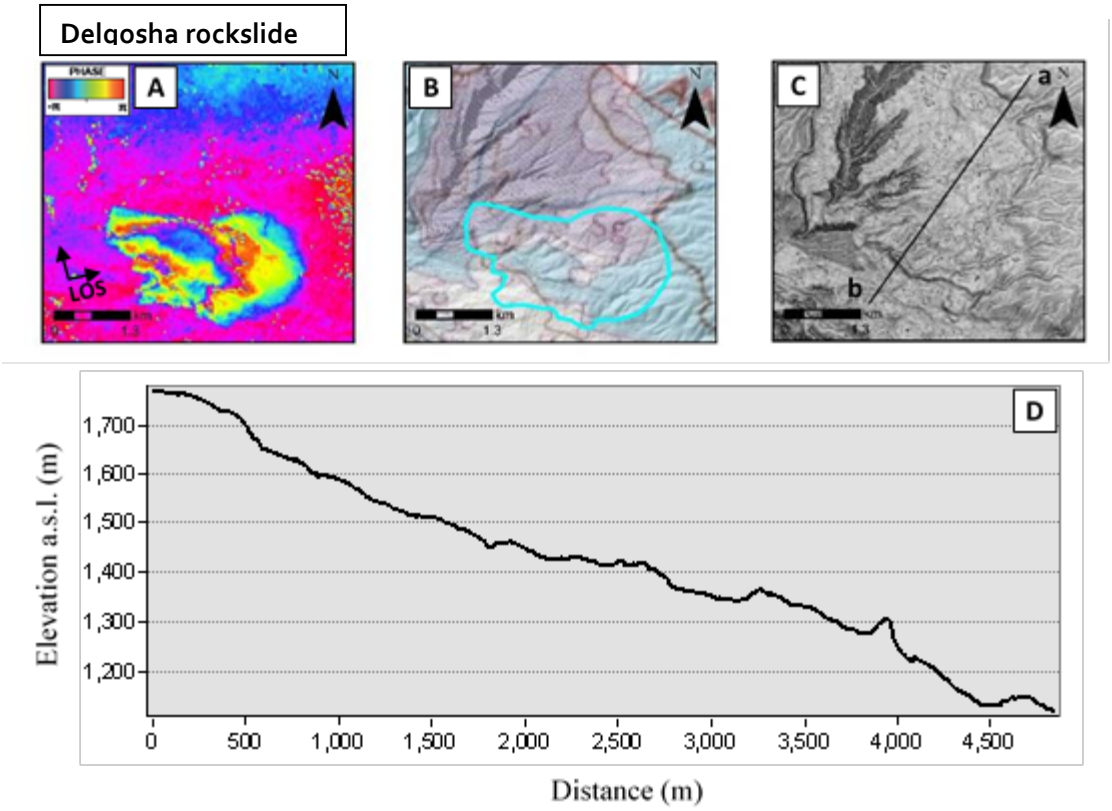
Delgosha rockslide
A
B
C
D
a
b
LOS
Elevation a.s.l. (m)
1,700
1,600
1,500
1,400
1,300
1,200
0
500
1,000
1,500
2,000
2,500
3,000
3,500
4,000
4,500
Distance (m)

183

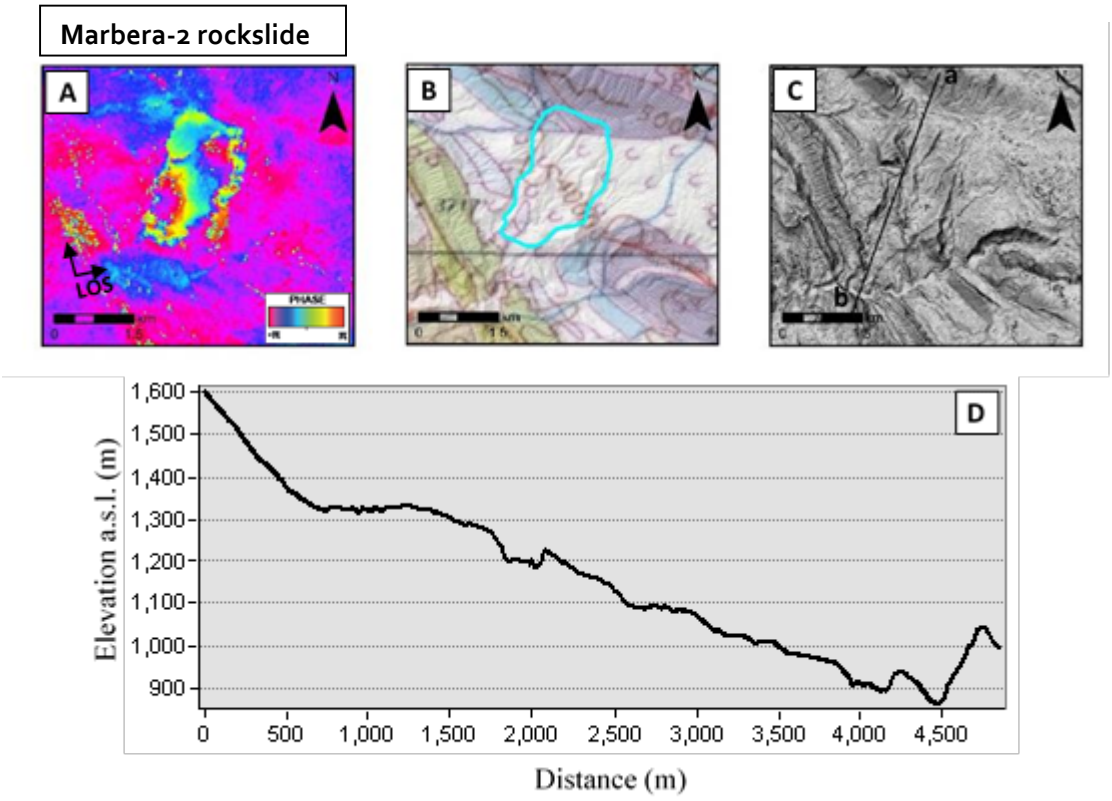
Marbera-2 rockslide
A
B
C
D
a
b
LOS
Elevation a.s.l. (m)
1,600
1,500
1,400
1,300
1,200
1,100
1,000
900
0
500
1,000
1,500
2,000
2,500
3,000
3,500
4,000
4,500
Distance (m)

184

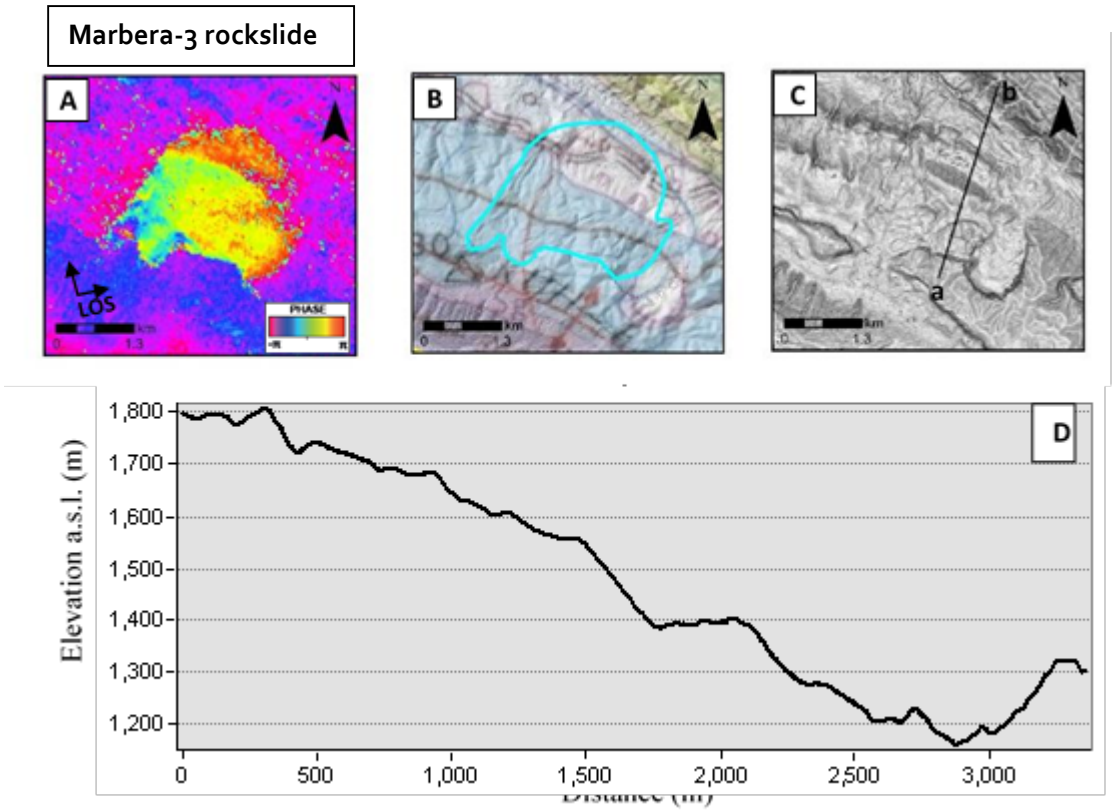
Marbera-3 rockslide
A
B
C
b
a
LOS
PHASE
D
Elevation a.s.l. (m)
1,800
1,700
1,600
1,500
1,400
1,300
1,200
0
500
1,000
1,500
2,000
2,500
3,000

185

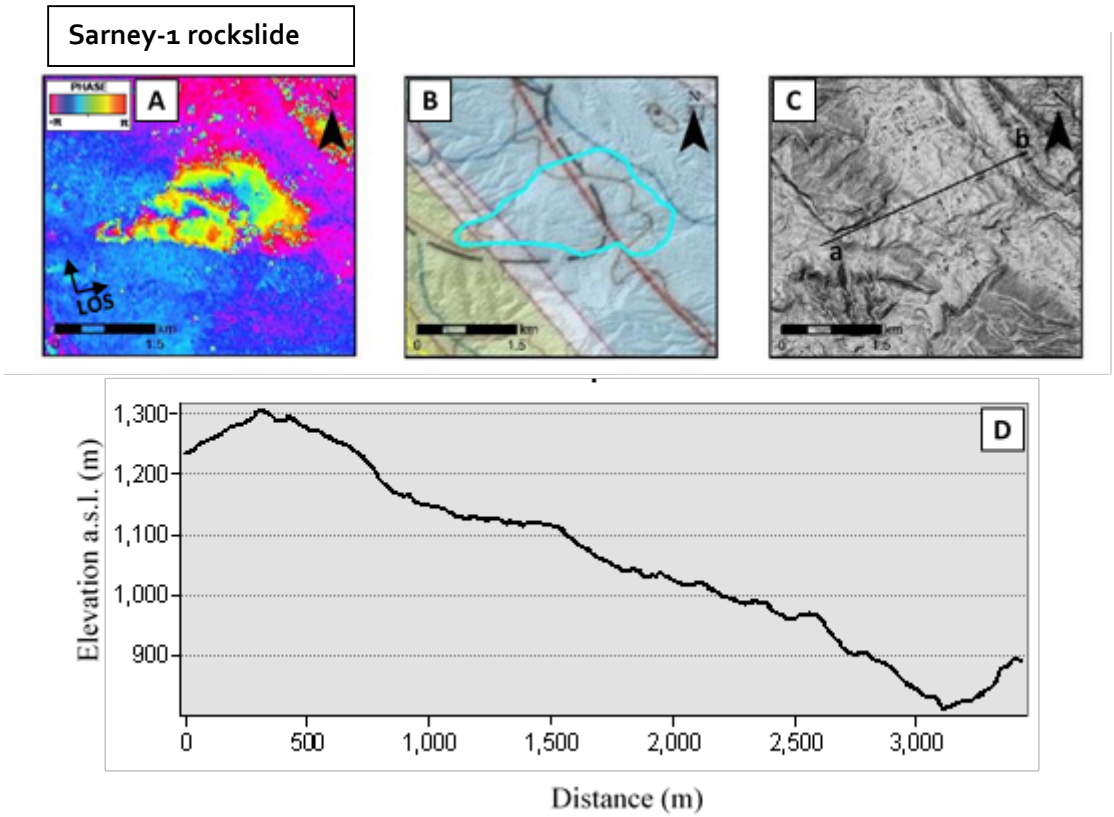
Sarney-1 rockslide
A
B
C
b
a
LOS
PHASE
D
Elevation a.s.l. (m)
1,300
1,200
1,100
1,000
900
0
500
1,000
1,500
2,000
2,500
3,000
Distance (m)

186

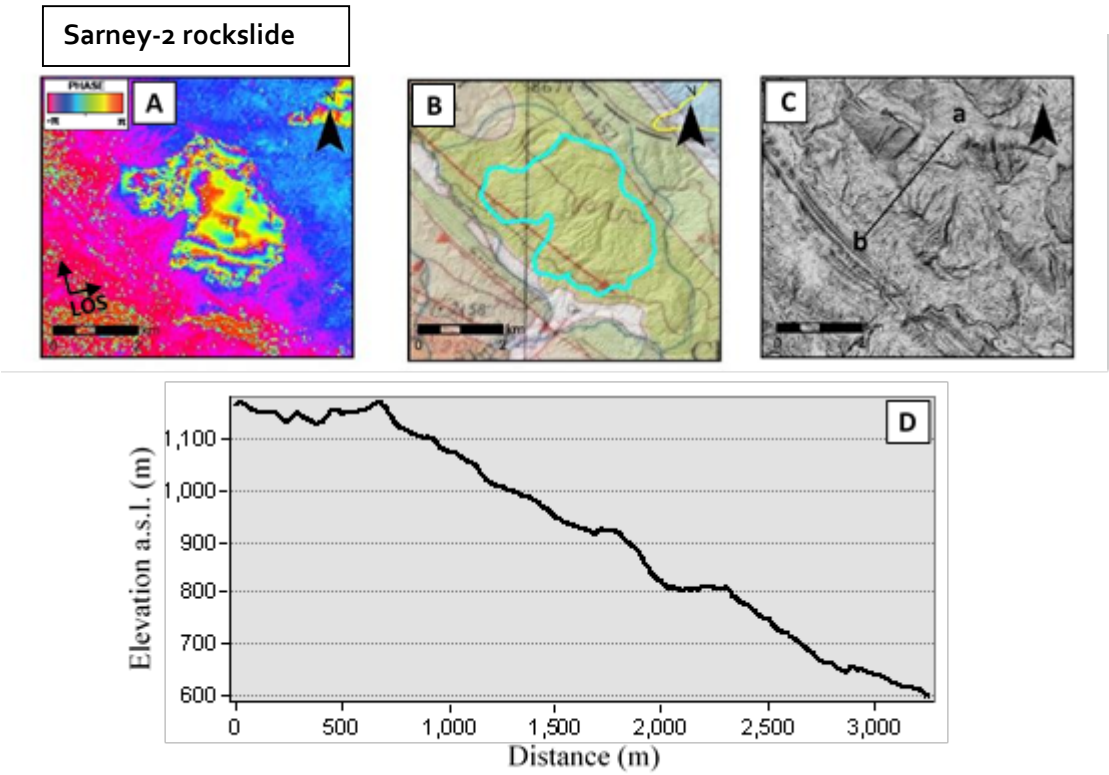

187

188 **Figure S6.** Figures showing (A) the interferogram pattern (the interferogram is computed
189 along the ascending track 72 between 11/11/2017 and 17/11/2017), (B) the geological map, (C)
190 the DEM and (D) a topographic profile 'ab' along the instance of the rockslides (other than the

191 Mehr rockslide). No detailed geological map is available for the region around the epicenter
192 (the region of the Bezmir-Abad and Mela-Kaboud landslide).

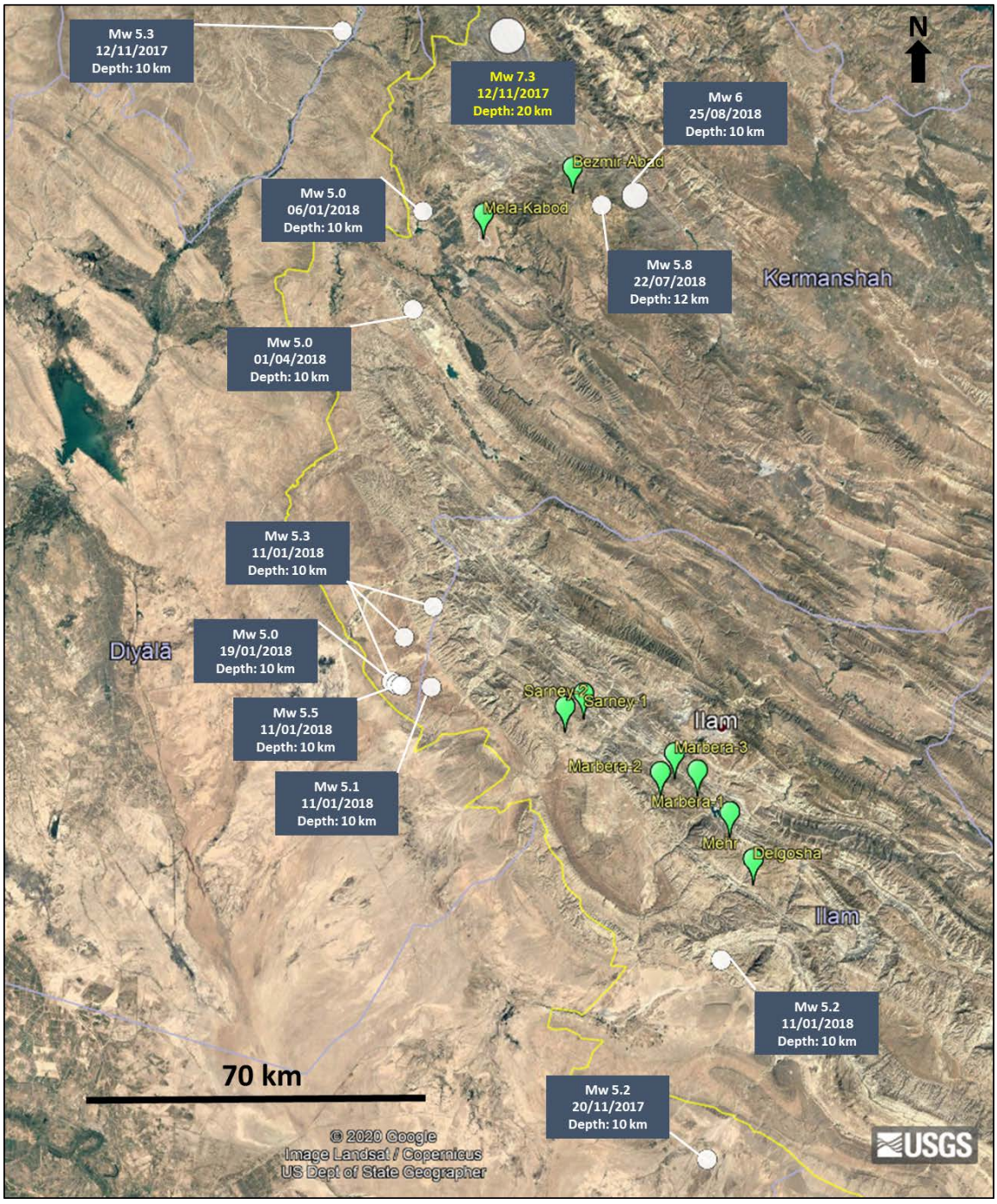

193

194 **Figure S7.** Details of all the seismic events that took place during the period of the
195 accomplished time-series analysis (10-01-2017 and 27-08-2018).

Data type and origin		Date of acquisition		Resolution (meter)	Application and use
		Pre-earthquake	Post-earthquake		
Optical	PlanetScope	19-Oct-2017 (North*)	13-Nov-2017 (North*)	3 m	-Image correlation (COSI-Corr) -Visual comparison
		07-Nov-2017 (South*)	17-Nov-2017 (South*)	3 m	
	Spot-6	13-Oct-2013, 24-Apr-2014 , 04-May-2014, 14-Aug-2014	29-Nov-2017 , 12-Dec-2017	1 m	-Image correlation (COSI-Corr) - Dem generation
Radar	Sentinel-1 AB	10-Jan-2017 to 06-Nov-2017 (repeat cycle each 12 days)	12-Nov-2017 to 27-Aug-2018 (repeat cycle each 12 days)	5x20 m	New Small BAseline Subset (NSBAS)
Digital Elevation Models	ASTER	----------		30 m	Correction of interferograms
	Spot-6/7	13-Oct-2013, 24-Apr-2014, 04-May-2014, 14-Aug-2014	29-Nov-2017, 12-Dec-2017	2 m	-Interpretation of landslides -Generation of cross-sections
		09-Nov-2014 (south*)		4 m	

North*correspond to the area around the epicenter

South* correspond to the area of the rockslides detected in the far field to the south from the epicenter

Table S1. Synthesis of satellite data used in this study and their characteristics.

Table S2. Characteristics of the giant slow-moving rockslides detected from Sentinel-1 interferograms and optical images correlation. The area of the rockslides already identified by Ghazipur and Simpson (2016) is given for comparison. The area deduced from this study

corresponds to the area of the interferogram (see Results for details). The volume is calculated based on the empirical law adopted in the study of Ghazipur and Simpson (2016) for the Zagros region. ΔH is the elevation difference between the landslide toe and its headscarp. The average slope is calculated from the headscarp top to the landslide toe. Landslide orientation gives the direction toward which the landslide is sliding; "North-East" means the landslide orientation is from South-West to North-East. Line Of Sight (LOS) velocities correspond to linear interpolation of accumulated displacements from time-series computed over several months (see Figure 4 and text S5 for details).